Coma morphology of comet 67P controlled by insolation over irregular nucleus

Xian Shi, Xuanyu Hu, Sefano Mottola, Holger Sierks, Horst Uwe Keller, Martin Rose, Carsten Guttler, Marco Fulle, Sonia Fornasier, Jessica Agarwal, et al.

LETTERS
https://doi.org/10.1038/s41550-018-0481-5

nature astronomy

Coma morphology of comet 67P controlled by insolation over irregular nucleus

X. Shi[1*], X. Hu[1,2], S. Mottola[3], H. Sierks[1], H. U. Keller[2,3], M. Rose[4], C. Güttler[1], M. Fulle[5], S. Fornasier[6], J. Agarwal[1], M. Pajola[7], C. Tubiana[1], D. Bodewits[8], C. Barbieri[9], P. L. Lamy[10], R. Rodrigo[11,12], D. Koschny[13], M. A. Barucci[6], J.-L. Bertaux[10], I. Bertini[9], S. Boudreault[1], G. Cremonese[14], V. Da Deppo[15], B. Davidsson[16], S. Debei[17], M. De Cecco[18], J. Deller[1], O. Groussin[19], P. J. Gutiérrez[20], S. F. Hviid[3], W.-H. Ip[21], L. Jorda[19], J. Knollenberg[3], G. Kovacs[1], J.-R. Kramm[1], E. Kührt[3], M. Küppers[22], L. M. Lara[20], M. Lazzarin[9], J. J. Lopez-Moreno[20], F. Marzari[9], G. Naletto[23,24,15], N. Oklay[3], I. Toth[25] and J.-B. Vincent[3]

While the structural complexity of cometary comae is already recognizable from telescopic observations[1], the innermost region, within a few radii of the nucleus, was not resolved until spacecraft exploration became a reality[2,3]. The dust coma displays jet-like features of enhanced brightness superposed on a diffuse background[1,4,5]. Some features can be traced to specific areas on the nucleus, and result conceivably from locally enhanced outgassing and/or dust emission[6–8]. However, diffuse or even uniform activity over topographic concavity can converge to produce jet-like features[9,10]. Therefore, linking observed coma morphology to the distribution of activity on the nucleus is difficult[11,12]. Here, we study the emergence of dust activity at sunrise on comet 67P/Churyumov–Gerasimenko using high-resolution, stereo images from the OSIRIS camera onboard the Rosetta spacecraft, where the sources and formation of the jet-like features are resolved. We perform numerical simulations to show that the ambient dust coma is driven by pervasive but non-uniform water outgassing from the homogeneous surface layer. Physical collimations of gas and dust flows occur at local maxima of insolation and also via topographic focusing. Coma structures are projected to exhibit jet-like features that vary with the perspective of the observer. For an irregular comet such as 67P/Churyumov–Gerasimenko, near-nucleus coma structures can be concealed in the shadow of the nucleus, which further complicates the picture.

In contrast to the occasional, short-lived outbursts, the nominal dust activity on comet 67P/Churyumov–Gerasimenko (hereafter 67P) varies distinctly with local time[8,10]. It begins instantly at sunrise along the dawn terminator[13], and follows the change of insolation through the day[14]. The diurnal variability suggests the dust emission is induced by volatile outgassing from the surface layers within the diurnal thermal skin depth. Before the perihelion passage in 2015, the abundances of highly volatile species, such as CO_2 and CO, in the coma over the northern hemi-nucleus were uncorrelated with insolation, evidently sourced from greater depths of the nucleus[15,16]. Water outgassing is left as the only plausible driver of nominal dust activity. The Hapi region connecting the two lobes of the nucleus[17,18] is known to be the source of the strongest water and dust activities before perihelion[19,20]. In Fig. 1a and b, we present two images taken by the OSIRIS (Optical, Spectroscopic, and Infrared Remote Imaging System) narrow-angle camera[21]. The observations were obtained on 22 August 2014 and 14 March 2015, at heliocentric distances of 3.4 au and 2.1 au, respectively (see Supplementary Fig. 1 and Supplementary Table 1 for viewing geometry and additional information of all observations used in this study). They show dust flows from the floor of the Hapi region at sunrise. The faint airborne dust, which is usually overwhelmed by the brightness of the illuminated nucleus, is projected vividly as 'jets' against the expansive and retreating shadows. These jet-like features have varying widths between ~10 m and ~50 m, and height between ~80 m and ~500 m. The apparent sources of the features appear to concur with bends

[1]Max-Planck-Institut für Sonnensystemforschung, Göttingen, Germany. [2]Institut für Geophysik und extraterrestrische Physik (IGEP), Technische Universität Braunschweig, Braunschweig, Germany. [3]Deutsches Zentrum für Luft- und Raumfahrt (DLR), Institut für Planetenforschung, Asteroiden und Kometen, Berlin, Germany. [4]PI-DSMC, Sindelfingen, Germany. [5]INAF - Osservatorio Astronomico, Trieste, Italy. [6]LESIA, Observatoire de Paris, PSL Research University, CNRS, Univ. Paris Diderot, Sorbonne Paris Cité, UPMC Univ. Paris 06, Sorbonne Universités, Meudon Principal Cedex, France. [7]NASA Ames Research Center, Moffett Field, CA, USA. [8]Department of Astronomy, University of Maryland, College Park, MD, USA. [9]Department of Physics and Astronomy, University of Padova, Padova, Italy. [10]Laboratoire Atmosphères, Milieux et Observations Spatiales, CNRS & Université de Versailles Saint-Quentin-en-Yvelines, Guyancourt, France. [11]Centro de Astrobiologia, CSIC-INTA, Madrid, Spain. [12]International Space Science Institute, Bern, Switzerland. [13]Scientific Support Office, European Space Research and Technology Centre/ESA, Noordwijk ZH, The Netherlands. [14]INAF, Osservatorio Astronomico di Padova, Padova, Italy. [15]CNR-IFN UOS Padova LUXOR, Padova, Italy. [16]Jet Propulsion Laboratory, Pasadena, CA, USA. [17]Department of Industrial Engineering, University of Padova, Padova, Italy. [18]University of Trento, Faculty of Engineering, Trento, Italy. [19]Aix Marseille Université, CNRS, LAM (Laboratoire d'Astrophysique de Marseille) UMR 7326, Marseille, France. [20]Instituto de Astrofísica de Andalucía -CSIC, Glorieta de la Astronomia, Granada, Spain. [21]Graduate Institute of Astronomy, National Central University, Chung-Li, Taiwan. [22]Operations Department, European Space Astronomy Centre/ESA, Villanueva de la Cañada (Madrid), Spain. [23]Department of Physics and Astronomy "G. Galilei", University of Padova, Padova, Italy. [24]Center of Studies and Activities for Space, CISAS, 'G. Colombo', University of Padova, Padova, Italy. [25]MTA CSFK Konkoly Observatory, Budapest, Hungary.
*e-mail: shi@mps.mpg.de

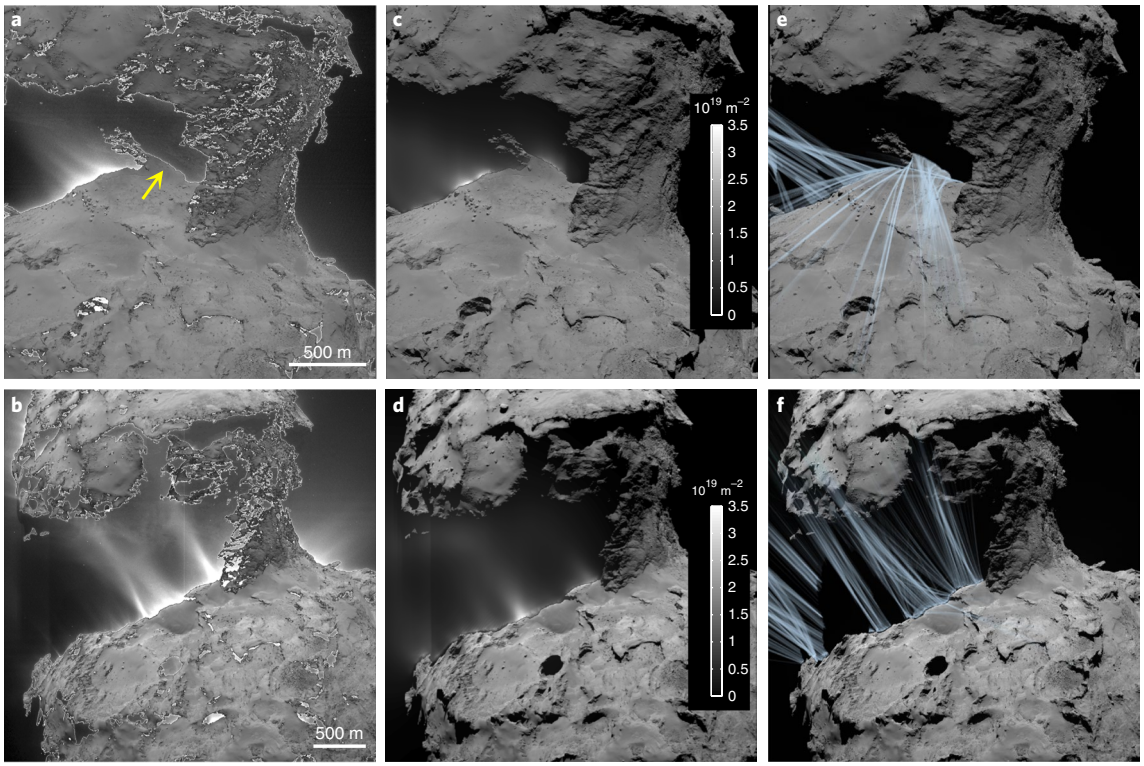

Fig. 1 | Observed and synthetic gas and dust emission from morning terminators on 67P. a,**b**, OSIRIS observations on 22 August 2014 and 14 March 2015 of jet-like features in the dust coma around dawn terminator in the Hapi region when 67P was at heliocentric distances of 3.5 and 2.1 au, respectively. The brightness contrasts of nucleus and coma are adjusted separately so that fine structures of both are visible. The yellow arrow in **a** points to the alcove at the transition from region Hapi to Hathor. **c**,**d**, Synthetic images showing modelled local water gas field developed from a strip of morning frost. The greyscale indicates modelled column density of water molecules. **e**,**f**, Trajectories of dust particles emitting from the terminator, moving in the modelled gas field shown in **c** and **d**.

and zigzags of the terminator, resulting from the abrupt topography or irregular shade cast by surrounding landscapes.

The source area displayed exposed, transient water ice, or morning frost, manifested in a strip of enhanced surface reflectance tracing the terminator compared with the adjacent long-lit surface (Supplementary Fig. 2). The diurnally recurring frost had been observed by VIRTIS, the Visible and Infrared Thermal Imaging Spectrometer onboard Rosetta[13]. It was formed by re-condensation of water vapour diffusing from the warm nucleus interior during the night, replenishing the ice content throughout the surface layers[13]. This diurnal water cycle was probably at work also on comet 103P/Hartley 2 (ref. [22]). The exposure of frost to the morning sun induces instant water outgassing and dust emission[13], a mechanism observed also on comet 9P/Tempel 1[23]. Morning frost observed on 67P only lasted for a few minutes after sunrise[24]. The water flux from the frosty surface layers in Hapi alone amounted to ~3% of the total water production rate of 67P (ref. [13]), a contribution similar to that from the exposed water ice on 9P/Tempel 1 (ref. [25]).

The emergence of activity from the frost induces an intrinsic, regular component of the diurnal coma morphology, as the terminator sweeps across the nucleus. We modelled the outgassing from the frost due to sublimation of the exposed ice by thermo-physical models developed for 67P[26,27] (see Methods for details of modelling). Using the modelled instantaneous surface temperature and outgassing flux as boundary conditions, we applied a three-dimensional direct simulation Monte Carlo (DSMC) method[28] to model the gas field sourced from the frost strip. The column densities of the modelled gas field in the same views as Fig. 1a and b are presented in greyscale in Fig. 1c and d, respectively. The gas fields are distinctly non-uniform. Jet-like features are visible whose brightness attenuates from the terminator. The bases of the simulated gas features are correlated with the locations of the observed dust flows, and the visual orientations of the gas and dust flows are consistent. In Fig. 1e and f we show the simulated motions of dust particles emitted from the terminator, subject to gas drag and nucleus gravity. The concentrations and scatters of the particle trajectories correspond to the pattern of gas column density and therefore mimic the observed dust coma morphology. In Fig. 1a, we note, in particular, the absence of dust features over an alcove (indicated by the yellow arrow) near the edge of the shadow in contrast to prominent activity along the rest of the terminator. As revealed in Fig. 1e, dust flows from there did not extend against the shadow at the time, but were instead overwhelmed by the brightness of the illuminated nucleus and therefore unobservable.

The presence of fine structures in the gas coma, with a pattern similar to that of dust is intriguing, considering the different dynamics of gas and dust[29]. The correlation between the patterns of the water and dust comae has been observed by VIRTIS, though on a scale of hundreds of metres to one kilometre[14,30]. Our simulation indicates that water gas coma can display fine jet-like structures and correlate with the dust coma at spatial scales as small as about 30 m. As shown in Fig. 2, the outgassing from the frosty strip formed a vapour curtain. At low altitudes, below 200 m above the surface for example, the number density of water vapour is inhomogeneous, giving rise to the collimation of flows or formation of gas jets (Fig. 2a). The mean free paths of the molecules are typically less than 10 m along the jets (Supplementary Fig. 3). The curtain expands and disperses outward from the nucleus (Fig. 2b,c). The gas jets nearly dissipate at about 800 m above the ground, where the contour of the curtain becomes indistinct (Fig. 2d).

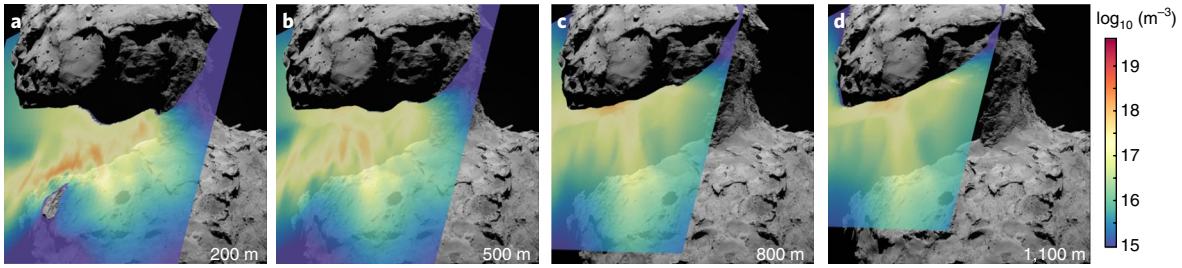

Fig. 2 | Number density of water molecules at different altitudes above the terminator. a–d, The number densities are sampled at cross-sections of the modelled gas coma parallel to a plane that best fits the terminator. The altitudes of the cross-sections are indicated at the bottom right of the respective panels.

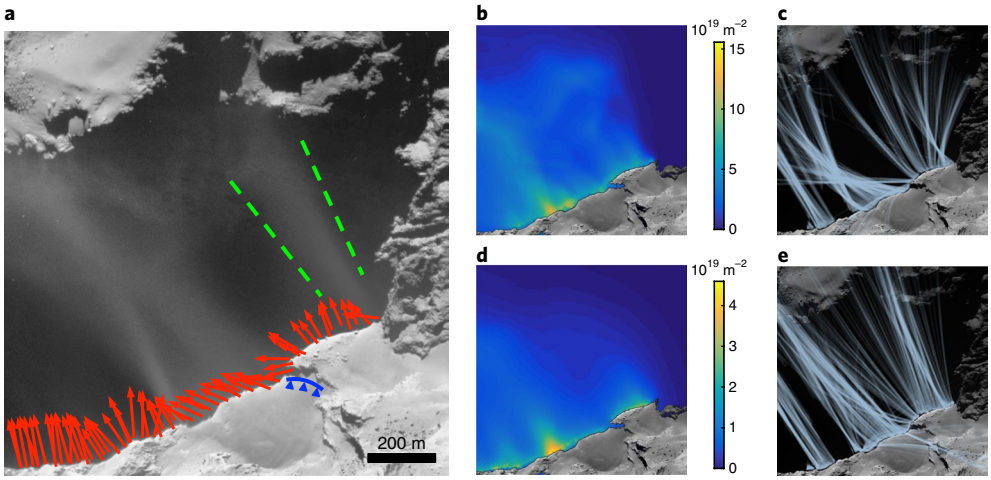

Fig. 3 | Influence of topography and outgassing flux on near-nucleus coma structure. a, Enlarged view of part of the observation in Fig. 1b, showing prominent dust jets along the dawn terminator. Red arrows indicate the normal direction of local surface along the terminator. The green dashed lines delimit one prominent jet close to the edge of the Hapi region. The blue solid line with arrowheads indicates the location of a small shadowed cliff on the terminator. **b**,**c**, Patterns of gas field and dust particle trajectories modelled with constant outgassing. **d**,**e**, Patterns of gas field and dust particle trajectories modelled with non-uniform outgassing driven by instant insolation. The colour scales in panels **b** and **d** indicate the column density of gas.

These physical corrugations of gas and dust densities occur under the following conditions. First, they result from the non-uniform water outgassing along the frosty terminator, which arises from varying sublimation rates of ice under different illumination conditions. Second, the curtain of gas and dust is effectively ruffled by topographic undulations. The prominent dust jets are associated with the sharp surface curvatures along the terminator and focused by concavities. In contrast, the curtain of ejecta is stretched thin over the convex surface areas, such that the coma became rarefied, displaying decreased brightness. The surface concavities and convexities thus naturally produce non-uniform coma structures even in the case of uniform water outgassing[10].

We distinguish the impact of topography on the coma structure from the influence of the local gas production rate by a simulation where we assumed constant outgassing flux from the terminator. As shown in Fig. 3b and c, it is clear that topography alone induces complex coma structures reminiscent of those in Fig. 3d and e. Strong collimations are always associated with 'converging' surface normals. Nevertheless, the morphology of the dust field clearly cannot be explained by topography alone. For example, a small cliff (indicated by the blue line and arrowheads in Fig. 3a) was in shadow hence clearly inactive at the time, which caused the relative sparsity of dust immediately above; while in the case of uniform outgassing, the gas flux from the cliff would have driven the dust flows in a more inclined direction over the surface (Fig. 3c). Another example is the prominent jet originating from the foot of the Hathor cliff (indicated by the green dashed lines in Fig. 3a). The effect of topography alone would result in scattered flows from the concavity. Instead, this jet was formed by locally stronger outgassing flux from the cliff floor. Here, the floor itself is slightly convex, and the surface near the cliff wall was less inclined toward the Sun and warmer by ~10 K than further away from the cliff, which results in a higher water flux by ~100%. Hence, the complex coma structures occur naturally around an irregularly shaped nucleus such as 67P. Not only does the landscape directly structure or collimate gas and dust flows, it also affects the diurnal alternations of illumination and, thus, the thermo-physical state of the nucleus' top-most layer[26,31,32].

In addition to thermo-physical conditions, the visual pattern of the near-nucleus dust coma depends strongly on the shadowing conditions and viewing geometry at the time of observation. In the case of 67P, shadows occur in a highly complex manner over the nucleus. In Fig. 1b, for instance, sunlight from the top is shielded from the Hapi region by the small lobe. The irregular umbrella produces cascading depths of the shadows, as manifested in several brightness terraces toward the limb of the nucleus on the left. The coma brightness against the shadow is highly uneven along the terminator and overall diminishes toward the left. The pattern does not indicate weakening of activity but reflects a visual effect, as the dust ejecta were driven into the shadow by the gas flows and, thus, could not be observed (as shown in Fig. 1f and Supplementary Fig. 4). It is interesting to note that one fine jet from the terminator penetrated through the thin shadow near the limb and brightened somewhat when it diffused into sunlight (Supplementary Fig. 5).

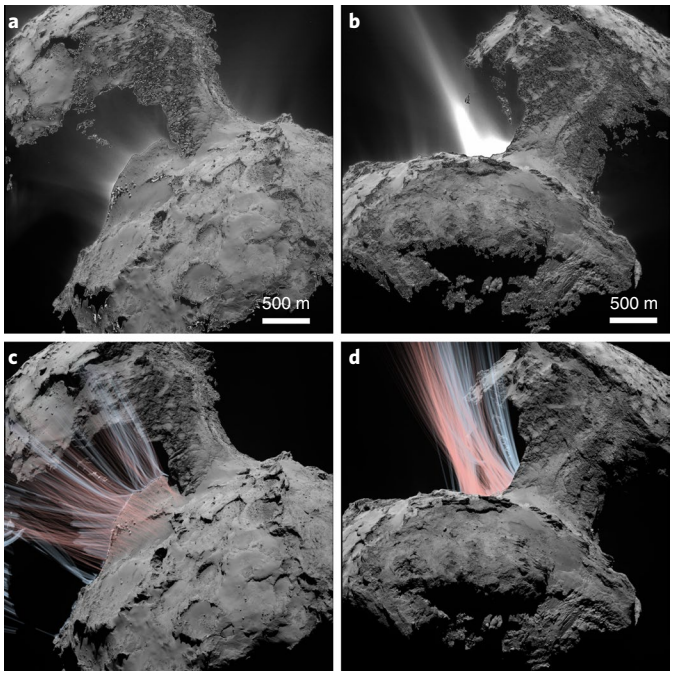

Fig. 4 | Dust coma in the neck region at the same local time but observed from different perspectives. a,**b**, Dust coma imaged from facing the neck valley and along the neck valley, respectively. **c**,**d**, Simulated dust particle trajectories for **a** and **b**, respectively, by taking into account gas field from the entire Hapi region. The blue tracks represent trajectories of dust particles emitted from the terminator, and the red tracks represent those from the rest of the illuminated area in Hapi.

Such complex shadowing effect on airborne dust confirms that the ejecta originated from the terminator frost, since dust in the foreground ejected from the long-lit areas would not have been shadowed.

A full characterization of the coma structure in three dimensions requires stereo observations of the instantaneous coma acquired in distinct viewing geometries. The dust coma of 67P exhibits diurnal repetition in OSIRIS observations[8], making it possible to repetitively observe the coma roughly unvaried over a few rotations of the nucleus. The set of images in Fig. 4 were taken six comet rotations apart and provide nearly orthogonal perspectives of the same dust coma under identical illumination conditions. Figure 4a shows an observation with a similar viewing geometry to those in Fig. 1. The pattern of coma brightness over the Hapi region was dominated by corrugations of the dust emerging along the terminator, whereas the contribution from the illuminated foreground appeared to be secondary (Fig. 4a). This is confirmed by the gradual shadowing of dust lifted from the terminator (blue trajectories in Fig. 4c). However, when the coma was viewed from the edge, the fine filaments as well as the corresponding modelled dust trajectories became indistinguishable and fuse into a prominent 'jet' (Fig. 4b,d). In this observation, the main part of the beam is attributed to dust ejected from the illuminated foreground (red trajectories), rather than from the terminator (blue trajectories). Moreover, the higher brightness in Fig. 4b than observed in Fig. 4a results from superimposition of signals or higher column density of dust along the line of sight[26]. This is reflected by the denseness of simulated dust trajectories in Fig. 4d greater than that in Fig. 4c. Hence, the same physical coma structure can exhibit vastly dissimilar morphologies and brightness intensities in different views (see also Supplementary Video 1).

There is no simple relationship between the appearance of jet-like features in observations and the physical occurrence of jets. In the case of 67P, the jet-like features may indicate topographic concavity, elevated insolation, or distribution of nightly frost over the irregular nucleus, all related to a homogenous surface layer. While some are definitively collimated dust flows, we must always entertain the possibility that jet-like features are optical illusions that cannot be easily linked with the nucleus activity. Here, a combination of elaborate image processing and application of state-of-the-art physical models proves to be necessary to obtain a clear picture of the structure and formation of cometary comae. The wealth of observations from Rosetta and beyond awaits further, in-depth analyses to better understand how comets work.

Methods

Near-nucleus gas field modelling. The motion of water molecules in the vicinity of the nucleus is modelled on a three-dimensional structured grid using the method of direct simulation Monte Carlo (DSMC)[33], realized with the software package of PI-DSMC. We adopt a local shape model with a lateral resolution of roughly 30 m (ref. [34]). For a given observation time, we determine the position of the morning terminator by simulating the illumination condition of each facet on the boundary surface.

We chose the modelled terminator as facets immediately adjacent to the unilluminated part of the nucleus. Surface temperature T and the corresponding outgassing rate $Z(T)$ are calculated for these facets using a thermo-physical model depicting the sublimation of dust–ice mixture on the nucleus surface (the model A in ref. [26]). We assumed sublimation of dusty ice fulfils the following energy conservation:

$$Q_{\odot}+Q_{\mathrm{SH}}=\varepsilon\sigma T^{4}+Z(T)\mathcal{L}_{\mathrm{ice}}$$

$Q_{\odot}=r_{\odot}^{-2}(1-A_{\mathrm{B}})C_{\odot}\max(0,\sin\varphi_{\odot})$ is the energy input from solar irradiation, where $A_{\mathrm{B}}=0.01$ is the Bond bolometric albedo, $C_{\odot}=1,361\ \mathrm{Wm}^{-2}$ is the solar constant $\varphi_{\odot}$ is the elevation angle of the Sun. Shadowing due to surrounding landscape is taken into account; $r_{\odot}$ is the heliocentric distance in au. Q_{SH} is the energy input due to absorption of thermal radiation of the nucleus itself, or self-heating. $\varepsilon=0.9$ is the infrared emissivity, σ is the Stefan–Boltzmann constant and $\mathcal{L}_{\mathrm{ice}}$ is the latent sublimation heat of water ice. $Z(T)$ is evaluated as follows[35]:

$$Z(T)=P_{\mathrm{V}}\sqrt{\frac{\hat{m}}{2\pi k_{\mathrm{B}}T}}$$

where $\hat{m}$ is the molecular mass of water, k_{B} is the Boltzmann constant and $P_{\mathrm{V}}=3.56\times10^{12}exp\,(-6,141.67T^{-1})\mathrm{kg\ m^{-1}s^{-2}}$ is the saturation vapour pressure of water.

In the gas field modelling, water molecules hitting the nucleus surface are reflected diffusely. The velocity is chosen according to the velocity distribution that is defined by the surface temperature at the time of reflection. Alternatively, a fraction of the molecules hitting the surface can be absorbed. For an outgassing area, the absorption would reduce the effective outgassing rate and the reduction depends on the outgassing rate itself as the molecules need to be directed back to the surface by collisions in the gas phase. In regions where inactive parts of the surface are interacting with the gas flow, the absorption probably has a stronger influence on the gas flow. It was argued that, for near-nucleus gas field, an absorbing or reflecting surface does not make a significant difference to the modelling results[36].

Motion of dust particles. Trajectories of dust particles are calculated in the body-fixed coordinate frame of 67P as defined in ref. [37]. It is assumed that dust and gas are decoupled at the beginning of the trajectory, meaning that dust particles are not affecting the motion of gas molecules. We use Runge–Kutta[4,5] formulae for the integration of the particle trajectories. For each step, we take into account gravitational acceleration $\mathbf{a}_{\mathrm{g}}$, gas drag acceleration $\mathbf{a}_{\mathrm{d}}$, centrifugal and Coriolis accelerations $\mathbf{a}_{\mathrm{r}}$ and $\mathbf{a}_{\mathrm{c}}$, so that the total acceleration vector of a certain particle with a position vector $\mathbf{r}$ is defined as:

$$\ddot{\mathbf{r}}=\mathbf{a}_{\mathrm{g}}+\mathbf{a}_{\mathrm{d}}+\mathbf{a}_{\mathrm{r}}+\mathbf{a}_{\mathrm{c}}$$

The gravitational acceleration $\mathbf{a}_{\mathrm{g}}$ is derived using the polyhedral shape model consisting F triangular facets as[38]:

$$\mathbf{a}_{\mathrm{g}}=-\frac{GM}{V}\sum_{f=1}^{F}\hat{\mathbf{n}}_{f}\left(\sum_{e=1}^{3}\hat{\mathbf{n}}_{e}^{f}\cdot\mathbf{r}_{e}^{f}\cdot L_{e}-\hat{\mathbf{n}}_{f}\cdot\mathbf{r}_{f}\cdot\omega_{f}\right)$$

where $GM = 666.2\ \mathrm{m^3 s^{-2}}$ is the measured gravitational parameter of 67P (ref. [39]). $V = 18.8\ \mathrm{km^3}$ is the total volume of 67P (ref. [17]). $\hat{\mathbf{n}}_f$ is the surface normal vector of facet f. $\hat{\mathbf{n}}_e^f$ is the normal vector of edge e of facet f within the facet plane. $\mathbf{r}_e^f$ is a vector from the field point to an arbitrary point on edge e, and $\mathbf{r}_f$ is such vector to facet f. L_e is the gravitational potential of edge e, and ω_f is the solid angle formed by facet f viewed from the field point. To save computational time, we applied a shape model with reduced resolution of ~200 m (ref. [34]). The drag acceleration on a spherical dust particle with radius d is defined as[40]:

$$\mathbf{a}_\mathrm{d} = \frac{3C_\mathrm{d}\rho_\mathrm{g}}{8d\rho_\mathrm{d}} |\mathbf{v}_\mathrm{g} - \dot{\mathbf{r}}| (\mathbf{v}_\mathrm{g} - \dot{\mathbf{r}})$$

We use $C_\mathrm{d} = 2$ as the drag coefficient[41], ρ_g and $\mathbf{v}_\mathrm{g}$ are the local density and velocity of the gas field. We use $\rho_\mathrm{d} = 500\ \mathrm{kg\ m^{-3}}$ as the bulk density and $d = 100\ \mu\mathrm{m}$ as the diameter of a spherical dust particle. We further include the centrifugal and Coriolis accelerations $\mathbf{a}_\mathrm{r}$ and $\mathbf{a}_\mathrm{c}$ as:

$$\mathbf{a}_\mathrm{r} = -\boldsymbol{\omega} \times (\boldsymbol{\omega} \times \mathbf{r})$$

$$\mathbf{a}_\mathrm{c} = -2\,\boldsymbol{\omega} \times \dot{\mathbf{r}}$$

Here, $\boldsymbol{\omega} = 1.407 \times 10^{-4}$ rad $\mathrm{s^{-1}}$ is the angular velocity of 67P (ref.[37]).

Data availability. The data that support the plots within this paper and other findings of this study are available from the corresponding author upon reasonable request.

Received: 17 December 2017; Accepted: 24 April 2018;
Published online: 21 May 2018

References

1. Farnham, T. L. Coma morphology of Jupiter-family comets. *Planet. Space Sci.* **57**, 1192–1217 (2009).
2. Keller, H. U. et al. First Halley multicolour camera imaging results from Giotto. *Nature* **321**, 320–326 (1986).
3. Sagdeev, R. Z. et al. The spatial distribution of dust jets seen during the Vega 2 flyby. *Astron. Astrophys.* **187**, 835–838 (1987).
4. Belton, M. J. Cometary activity, active areas, and a mechanism for collimated outflows on 1P, 9P, 19P, and 81P. *Icarus* **210**, 881–897 (2010).
5. Farnham, T. L. et al. Connections between the jet activity and surface features on Comet 9P/Tempel 1. *Icarus* **222**, 540–549 (2013).
6. Yelle, R. V., Soderblom, L. A. & Jokipii, J. R. Formation of jets in Comet 19P/Borrelly by subsurface geysers. *Icarus* **167**, 30–36 (2004).
7. Combi, M. R. et al. Narrow dust jets in a diffuse gas coma: a natural product of small active regions on comets. *Astrophys. J.* **749**, 29 (2012).
8. Vincent, J. et al. Are fractured cliffs the sources of cometary dust jets? Insights from OSIRIS/Rosetta at 67P. *Astron. Astrophys.* **587**, A14 (2015).
9. Crifo, J. F., Rodionov, A. V., Szego, K. & Fulle, M. Challenging a paradigm: do we need active and inactive areas to account for near-nuclear jet activity? *Earth Moon Planets* **90**, 227–238 (2002).
10. Kramer, T. & Noack, M. On the origin of inner coma structures observed by Rosetta during a diurnal rotation of comet 67P/Churyumov-Gerasimenko. *Astrophys. J.* **823**, L11 (2016).
11. Crifo, J. F., Fulle, M., Kömle, N. I. & Szego, K. in *Comets II* 471–503 (The University of Arizona Press, Tucson, 2004).
12. Fulle, M. et al. Unexpected and significant findings in comet 67P/Churyumov-Gerasimenko: an interdisciplinary view. *Mon. Not. R. Astron. Soc.* **462**, S2–S8 (2016).
13. De Sanctis, M. C. et al. The diurnal cycle of water ice on comet 67P/Churyumov-Gerasimenko. *Nature* **525**, 500–503 (2015).
14. Rinaldi, G. et al. Properties of the dust in the coma of 67P/Churyumov–Gerasimenko observed with VIRTIS-M. *Mon. Not. R. Astron. Soc.* **462**, 547–561 (2016).
15. Hässig, M. et al. Time variability and heterogeneity in the coma of 67P/Churyumov-Gerasimenko. *Science* **347**, aaa0276 (2015).
16. Fougere, N. et al. Direct Simulation Monte Carlo modelling of the major species in the coma of comet 67P/Churyumov-Gerasimenko. *Mon. Not. R. Astron. Soc.* **462**, 156–169 (2016).
17. Sierks, H. et al. On the nucleus structure and activity of comet 67P/Churyumov-Gerasimenko. *Science* **347**, aaa1044 (2015).
18. Thomas, N. et al. The morphological diversity of comet 67P/Churyumov-Gerasimenko. *Science* **347**, aaa0440 (2015).
19. Lara, L. M. et al. Large-scale dust jets in the coma of 67P/Churyumov-Gerasimenko as seen by the OSIRIS instrument onboard Rosetta. *Astron. Astrophys.* **583**, A9 (2015).
20. Lin, Z.-Y. et al. Morphology and dynamics of jets of comet 67P/Churyumov-Gerasimenko: early phase development. *Astron. Astrophys.* **583**, A11 (2015).
21. Keller, H. U. et al. OSIRIS - the scientific camera system onboard Rosetta. *Space Sci. Rev.* **128**, 433–506 (2007).
22. Sunshine, J. M. et al. Water ice on comet 103P/Hartley 2. *EPSC-DPS Joint Meeting 2011* abstr. 1345 (2011).
23. Prialnik, D., A'Hearn, M. F. & Meech, K. J. A mechanism for short-lived cometary outbursts at sunrise as observed by Deep Impact on 9P/Tempel 1. *Mon. Not. R. Astron. Soc.* **388**, L20–L23 (2008).
24. Fornasier, S. et al. Rosetta's comet 67P/Churyumov-Gerasimenko sheds its dusty mantle to reveal its icy nature. *Science* **354**, 1566–1570 (2016).
25. Sunshine, J. M. et al. Exposed water ice deposits on the surface of comet 9P/Tempel 1. *Science* **311**, 1453–1455 (2006).
26. Keller, H. U. et al. Insolation, erosion, and morphology of comet 67P/Churyumov-Gerasimenko. *Astron. Astrophys.* **583**, A34 (2015).
27. Hu, X. et al. Thermal modeling of water activity on comet 67P/Churyumov-Gerasimenko with global dust mantle and plural dust-to-ice ratio. *Mon. Not. R. Astron. Soc.* **469**, 295–311 (2017).
28. Rose, M. Simulation of a complete triple turbo molecular pumping stage using direct simulation Monte Carlo in 3D. *AIP Conf. Proc.* **1628**, 212–219 (2014).
29. Huebner, W. F. et al. *Heat and Gas Diffusion in Comet Nuclei* ISSI Scientific Report SR-004 (International Space Science Institute, Bern, 2006).
30. Migliorini, A. et al. Water and carbon dioxide distribution in the 67P/Churyumov-Gerasimenko coma from VIRTIS-M infrared observations. *Astron. Astrophys.* **589**, A45 (2016).
31. Shi, X. et al. Sunset jets observed on comet 67P/Churyumov-Gerasimenko sustained by subsurface thermal lag. *Astron. Astrophys.* **586**, A7 (2016).
32. Hu, X. et al. Seasonal erosion and restoration of the dust cover on comet 67P/Churyumov-Gerasimenko as observed by OSIRIS onboard Rosetta. *Astron. Astrophys.* **604**, A114 (2017).
33. Bird, G. A. *Molecular Gas Dynamics and the Direct Simulation Monte Carlo of Gas Flows* (Clarendon Press, Oxford, 1994).
34. Jorda, L. et al. The global shape, density and rotation of Comet 67P/Churyumov-Gerasimenko from preperihelion Rosetta/OSIRIS observations. *Icarus* **277**, 257–278 (2016).
35. Fanale, P. & James Salvail, R. An idealized short-period comet model: surface insolation, H_2O flux, dust flux, and mantle evolution. *Icarus* **60**, 476–511 (1984).
36. Marschall, R. et al. Modelling observations of the inner gas and dust coma of comet 67P/Churyumov-Gerasimenko using ROSINA/COPS and OSIRIS data: first results. *Astron. Astrophys.* **589**, A90 (2016).
37. Preusker, F. et al. Shape model, reference system definition, and cartographic mapping standards for comet 67P/Churyumov-Gerasimenko – stereo-photogrammetric analysis of Rosetta/OSIRIS image data. *Astron. Astrophys.* **583**, A33 (2015).
38. Werner, R. A. & Scheeres, D. J. Exterior gravitation of a polyhedron derived and compared with harmonic and mascon gravitation representations of asteroid 4769 Castalia. *Celest. Mech. Dyn. Astr.* **65**, 313–344 (1997).
39. Pätzold, M. et al. A homogeneous nucleus for comet 67P/Churyumov-Gerasimenko from its gravity field. *Nature* **530**, 63–65 (2015).
40. Grün, E. et al. Mechanisms of dust emission from the surface of a cometary nucleus. *Adv. Space Res.* **9**, 133–137 (1989).
41. Gombosi, T. I., Nagy, A. F. & Gravens, T. E. Dust and neutral gas modeling of the inner atmospheres of comets. *Rev. Geophys.* **24**, 667–700 (1986).

Acknowledgements

OSIRIS was built by a consortium led by the Max-Planck-Institut für Sonnensystemforschung, Göttingen, Germany, in collaboration with CISAS, University of Padova, Italy, the Laboratoire d'Astrophysique de Marseille, France, the Instituto de Astrofísica de Andalucia, CSIC, Granada, Spain, the Scientific Support Office of the European Space Agency, Noordwijk, The Netherlands, the Instituto Nacional de Técnica Aeroespacial, Madrid, Spain, the Universidad Politéchnica de Madrid, Spain, the Department of Physics and Astronomy of Uppsala University, Sweden, and the Institut für Datentechnik und Kommunikationsnetze der Technischen Universität Braunschweig, Germany. The support of the national funding agencies of Germany (DLR), France (CNES), Italy (ASI), Spain (MEC), Sweden (SNSB) and the ESA Technical Directorate is gratefully acknowledged.

Author contributions

X.S. led this study, analysed imaging data, performed simulations for gas and dust field modelling, and drafted the manuscript. X.H. contributed to design of the study, performed part of the thermo-physical analysis and contributed to drafting the manuscript. S.M. contributed to the thermo-physical modelling of water activity along dawn terminator and contributed to improving the manuscript. M.R. carried out the development and modification of DSMC code used for cometary coma modelling.

H.U.K. and M.F. contributed to interpretation of the results. H.S., C.G. and C.T. participated in early discussions of the study and helped improve the manuscript. S.F., M.P., J.A. and D.B. contributed to improving the manuscript. All remaining authors contributed to the construction, operation and calibration of OSIRIS cameras, which ensured the acquirement of high-quality data used for this study.

Competing interests

The authors declare no competing interests.

Additional information

Supplementary information is available for this paper at https://doi.org/10.1038/s41550-018-0481-5.

Reprints and permissions information is available at www.nature.com/reprints.

Correspondence and requests for materials should be addressed to X.S.

Publisher's note: Springer Nature remains neutral with regard to jurisdictional claims in published maps and institutional affiliations.